

NORSAR

ROYAL NORWEGIAN COUNCIL FOR SCIENTIFIC AND INDUSTRIAL RESEARCH

Scientific Report No. 2-85/86

SEMIANNUAL TECHNICAL SUMMARY

1 October 1985 – 31 March 1986

L.B. Loughran (ed.)

Kjeller, May 1986



APPROVED FOR PUBLIC RELEASE, DISTRIBUTION UNLIMITED

VII.6 Wavefield decomposition using ML-probabilities in modelling single-site 3-component records

This topic was dealt with in the previous NORSAR Semiannual Technical Summary, and a comprehensive write-up of the theoretical framework for this approach has now been completed (e.g., see Christoffersson et al, 1986). In this section, we will discuss some principal features of this novel analyzing technique, particularly those of importance for practical applications which will be demonstrated in subsequent sections.

Time vis-à-vis frequency domain analysis

So far our preference has been for time domain analysis, as good time resolution is achievable (window length 1-2 cycles), while the relative bandwidth is sufficiently broad to dampen the adverse effects of unstable narrow-band spectral estimates, particularly when short time windows are used. We have in fact not explored frequency domain analysis, although a practical advantage here is that the observational degrees of freedom would be 6 + 6 (amplitude and phase), while in the time domain we have only 6 (amplitude). Olson and Samson (1979) have demonstrated potential advantages of frequency domain operation for event detection.

Particle motion modelling

With only 6 observational degrees of freedom available (symmetric covariance matrix), particle motion modelling for P, SV, SH, L (Love) and R (Rayleigh) must be simple, and in this respect we follow standard approaches. The crucial question is naturally whether these models are adequate in practice, particularly in view of the well-documented wave propagation complexities for crustal phases (e.g., see Kennett, 1983). On the basis of extensive 3-component analysis of real data (NORESS records), the following comments apply.

P-waves: Few problems are encountered here. P-wavelets are easily identified as such, and very good slowness estimates are obtainable. Azimuth estimates are within ± 5 deg of true ones (for LP data often within ± 2 deg), and apparent velocity within ± 2 km s⁻¹. For small events, say for SNRs less than 2, larger estimation errors may ensue, although a suite of slownesses for several wavelets often provide good average estimates.

Shear waves: These waves are very important for locating events because P-S differential travel times provide reliable estimates of epicentral distances for broadband recordings and short period recordings at regional distances. However, S-waves are far more complex than P because mode conversions, reflections beyond critical angles, etc., produce non-linear particle motions. This is not incorporated in the model, so χ^2 -tests on S-wave presence often fail. Two strategies here are under consideration: i) more complex models entailing use of arrays of three-component stations and ii) simplifying the model from 3 to 2 dimensions, as triggering failures mainly reflect correlations between radial and transverse components. Regarding the first we have only experimented with simple stacking of the four 3-component stations with NORESS; besides improved SNR, this does not solve the "problem". In the second case, reliable S-wave identification occurs, but the penalty is loss of azimuth resolution. For calculating differential travel times (and epicentral distances), this is not a severe drawback.

R- and L-waves: We have relatively little experience in analysis (mostly of the Sg/Lg-wavetrain) and the problems encountered for S-waves appear to prevail here as well -- 2-D modelling is under consideration.

False alarms -- noise directionality

It is well known from array operations that the false alarm rate (noise wavelet triggering) to some extent reflects the structure of the noise field. Such phenomena are well known for NORSAR, that is, the false alarm rate increases for relatively monochromatic noise, as is the case during periods of strong coastal surfs (e.g., see Steinert et al, 1975). Such phenomena are seen in the NORESS detection log, but for this array such problems are more interesting. For example, Ingate et al (1985) found that the noise correlation (as a function of sensor separation) is somewhat different for horizontal and vertical travelling waves, which was attributed to the so-called "whispering" mantle effect or P-wave reverberations in the mantle. Also, the large dynamic range (120 dB) in the NORESS recording system implies that local operations like heavy machinery, hydroelectric power stations, etc., may temporarily constitute localized noise sources. An example here is given in Fig. VII.6.1, where semblance analysis implies a sort of beat phenomenon at 100 deg azimuth and velocity 2.8 km s^{-1} . We associated this with the Braskereid power station in the river Glomma and coinciding with the spring flooding. In 3-component analysis we see parts of the Rayleigh waves as vertical travelling P-waves, apparently because the horizontal part of R is lost in the noise. The Hunderfossen power station ($\Delta \sim 67 \text{ km}$, $Az = 330 \text{ deg}$) also seems to act as a noise source; in the 3-component analysis we see it as Pg-travelling waves in the azimuth section 300-360 deg. The Hunderfossen "noise source" has also been seen in NORSAR analysis (e.g., see Nikolaev and Troitskiy, 1986).

Structural complexities beneath NORESS

The essence of wavefield decomposition analysis is simply to identify wavelets of a specific type, and then provide estimates of the associated slowness vector. Apparent velocity applies only to P- and SV-waves. There is naturally an important problem in separating random

and deterministic scattering sources, but a puzzling feature at NORESS is that transverse (SH) motion occasionally is seen in the middle of the teleseismic P-wavetrains as illustrated in Fig. VII.6.2, but never at all four 3-component stations at the same time. This implies the existence of an anomalous body just beneath NORESS at a depth of around 15-20 km on the basis of P-S move-out times.

The traditional way of locating heterogeneous bodies beneath an array or network is that of inverting P travel time anomalies (e.g., see Aki et al, 1977, and Section VII.8). We are conducting this kind of experiments for NORESS, and preliminary results on the basis of travel time residuals for P waves are shown in Fig. VII.6.3. A 3-layered reference model was used; layer thicknesses of 1, 1.5 and 2.5 km, respectively, layer velocities were 5.8, 6.0 and 6.2 km s⁻¹, respectively, while the corresponding block sizes were 0.8, 1.0 and 1.2 km, respectively. The obtained velocity anomalies have a minimum range of ± 1.0 km s⁻¹, which in turn explained 60% of the variance in the observations. In this kind of experiment resolution decreases rapidly when layer depth greatly exceeds that of array aperture.

The next steps in our efforts to map heterogeneities beneath NORESS is that of amplitude inversion, and also to synthesize amplitude anomalies on the basis of derived velocity anomalies.

3-component analysis results -- displays in easily interpretable manner

A common problem for the many techniques developed for analysis of 3-component records, that is, exploiting the wavefield structure, is that the results are not displayed in an easily interpretable manner. Often rather messy particle motion plots, records distorted by non-linear rectilinear filtering, etc., apparently is no answer to this kind of problem. In our approach results are displayed in terms of χ^2 -probabilities (or apparent velocity for P when relevant), as a function of time and azimuth as illustrated in Fig VII.6.4. In the

upper part, the original and filter records are displayed (Z, Transverse, Radial components for a given azimuth), together with their filtered versions. The filtering is a simple weighting operation using the estimated probabilities (peak values) within a given azimuth band. Further refinements are feasible, that is, by only accepting probabilities associated with a given velocity range. For example, in this way we may exclude crustal reverberations (Pg-contributions) when analyzing teleseismic events.

Typical window lengths are one/two cycles, time increment 1/3 or 1/2 of this, azimuth increment 0.5-2.0 deg, and the records themselves are bandpass filtered (zero phase shift) prior to analysis when needed. Parameterized analysis results are easily extractable using interactive graphics (IBM PC/AT) combined with cursor usage. So far, this is restricted to wavelet onset time and corresponding azimuth, velocity and probability, the essential parameters for epicenter locations.

The last question to be addressed in this section is how well does our novel 3-component analysis technique work for poor SNRs. It is difficult to give a simple answer to this problem, but in a number of cases 3-component analysis of stacked records (the 4 stations A0, C2, C4 and C7) provide phase identification of weak signals not seen or not easily seen in the NORESS beam records. In other cases the array would detect events which are probably not detectable by 3-component analysis.

Practical applications of 3-component analysis

Besides the scattering study described previously (Dainty and Husebye, 1986), our main application of our 3-component analysis technique has been in parameter extraction for epicenter locations at local,

regional and teleseismic distances. These topics are dealt with in Section VII.7.

E.S. Husebye
B.O. Ruud
A. Christoffersson, Univ. of
Uppsala

References

- Aki, K., A. Christoffersson & E.S. Husebye (1977): Determination of the 3-dimensional seismic structure of the lithosphere. *J. Geophys. Res.*, 82, 277-296.
- Christoffersson, A., E.S. Husebye & S.F. Ingate (1986): Wavefield decomposition using ML-probabilities in modelling single-site 3-component records, *Geophys. J. R. astr. Soc.*, submitted for publication.
- Ingate, S.F., E.S. Husebye & A. Christoffersson (1985): Regional arrays and optimum data processing schemes. *Bull. Seism. Soc. Am.*, 75, 1155-1177.
- Kennett, B.L.N. (1983): *Seismic Wave Propagation in Stratified Media*. Cambridge Univ. Press.
- Nikolaev, A.V. & P.A. Troitskiy (1986): The earth structure study by means of seismic noise: Method, results and prospects. *Phys. Earth Planet. Inter.*, in press.
- Olson, J.V. & J.C. Samson (1979): On the detection of the polarization states of Pc micropulsations. *Geophys. Res. Lett.*, 6, 413-416.
- Steinert, O., E.S. Husebye & H. Gjøystdal (1975): Event detection false alarm rate and noise stability at NORSAR. *J. Geophys. Res.*, 41, 289-302.

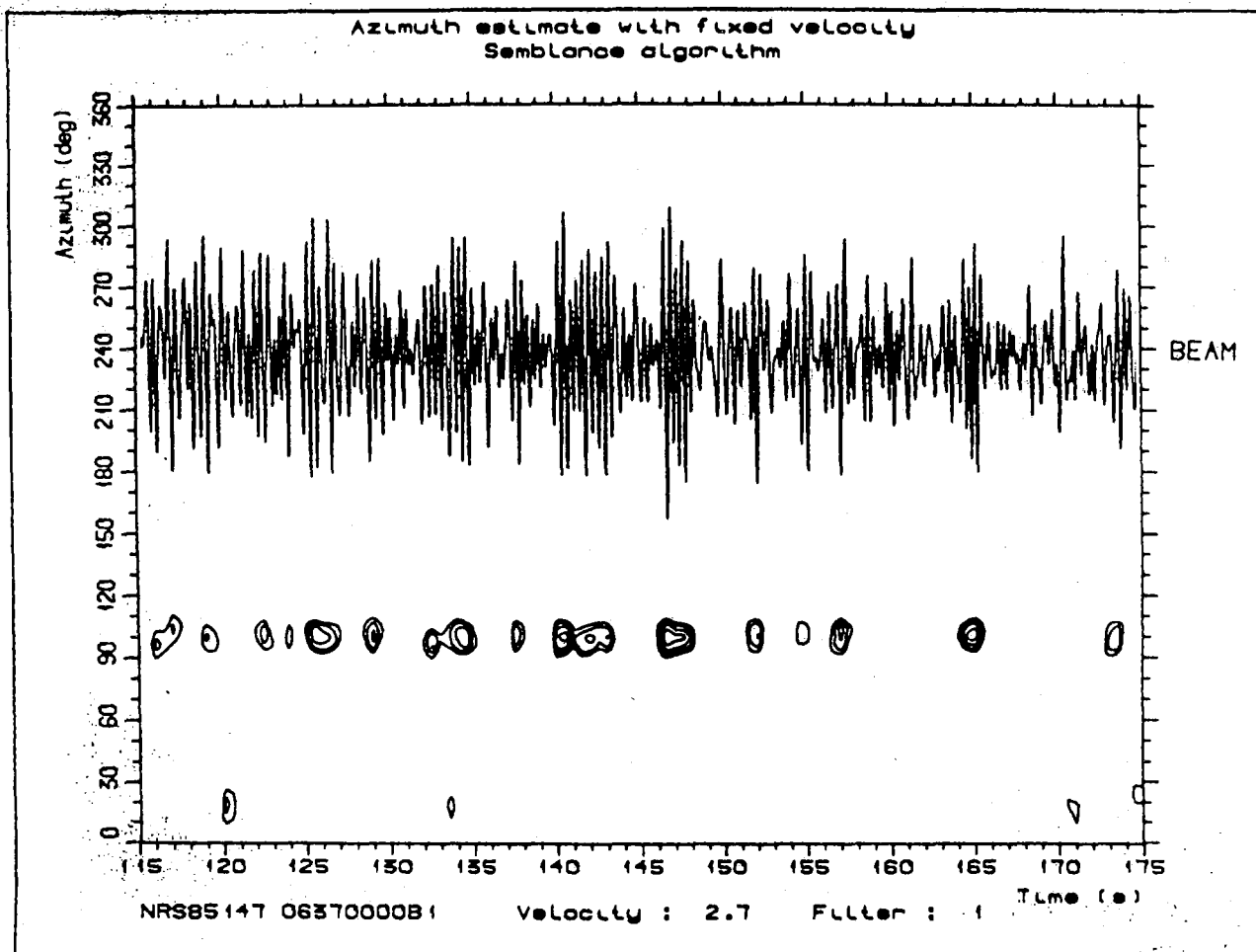


Fig. VI.6.1 Noise directionality as illustrated from presumed vibrations at Braskereidfoss power station at 06.47, 27 May 1985 (spring flooding in river Glomma). Semblance analyzed used with $vel = 2.7 \text{ km s}^{-1}$; triggering occurred only at $az \approx 100 \text{ deg}$. The associated beam wavelets are also displayed. Such effects are also manifested in the NORESS detection log, and naturally generate Pg-triggering in 3-component analysis.

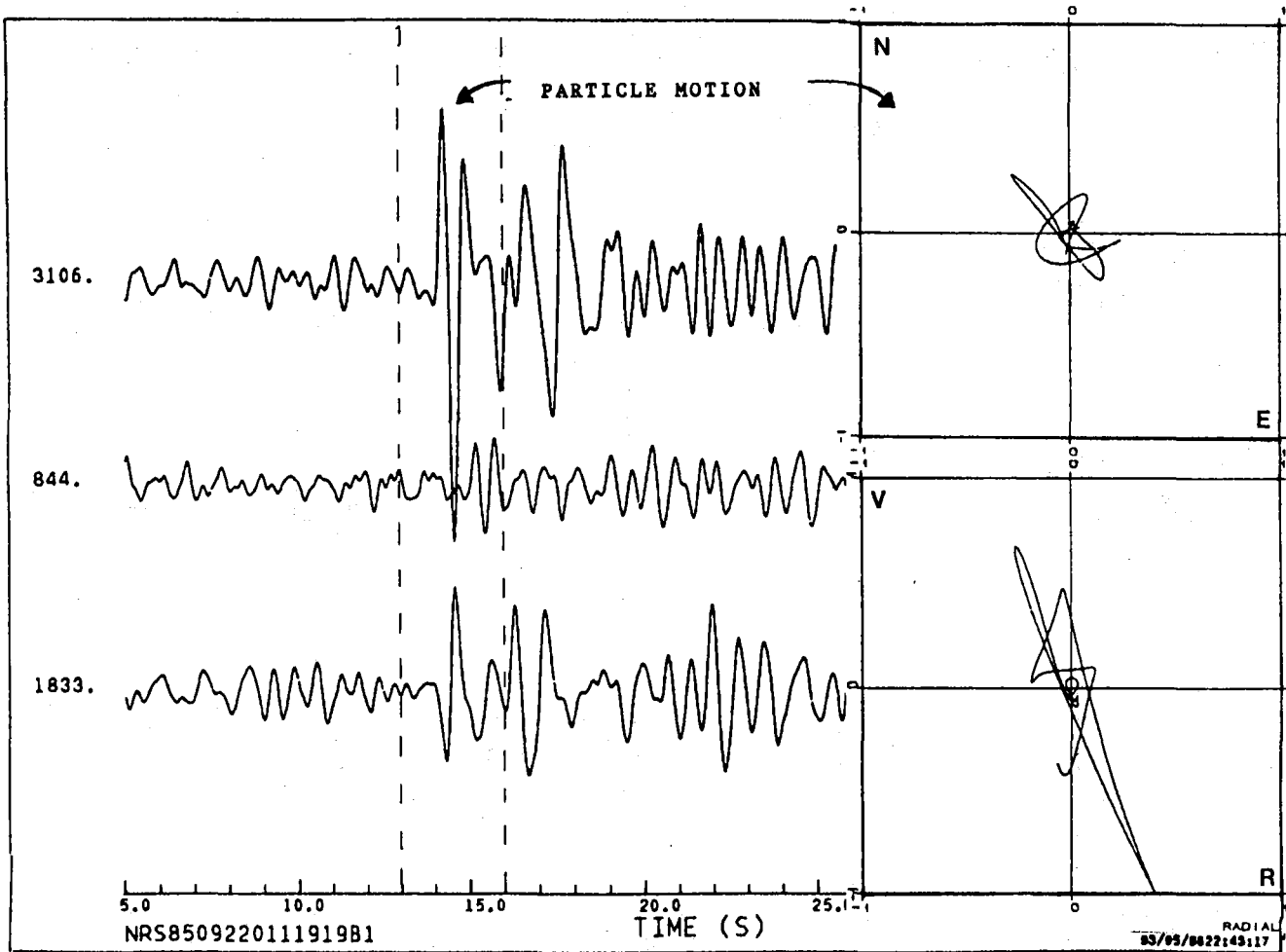


Fig. VII.6.2 Nevada explosion 2 April 1985. SV-presence in the P signal.

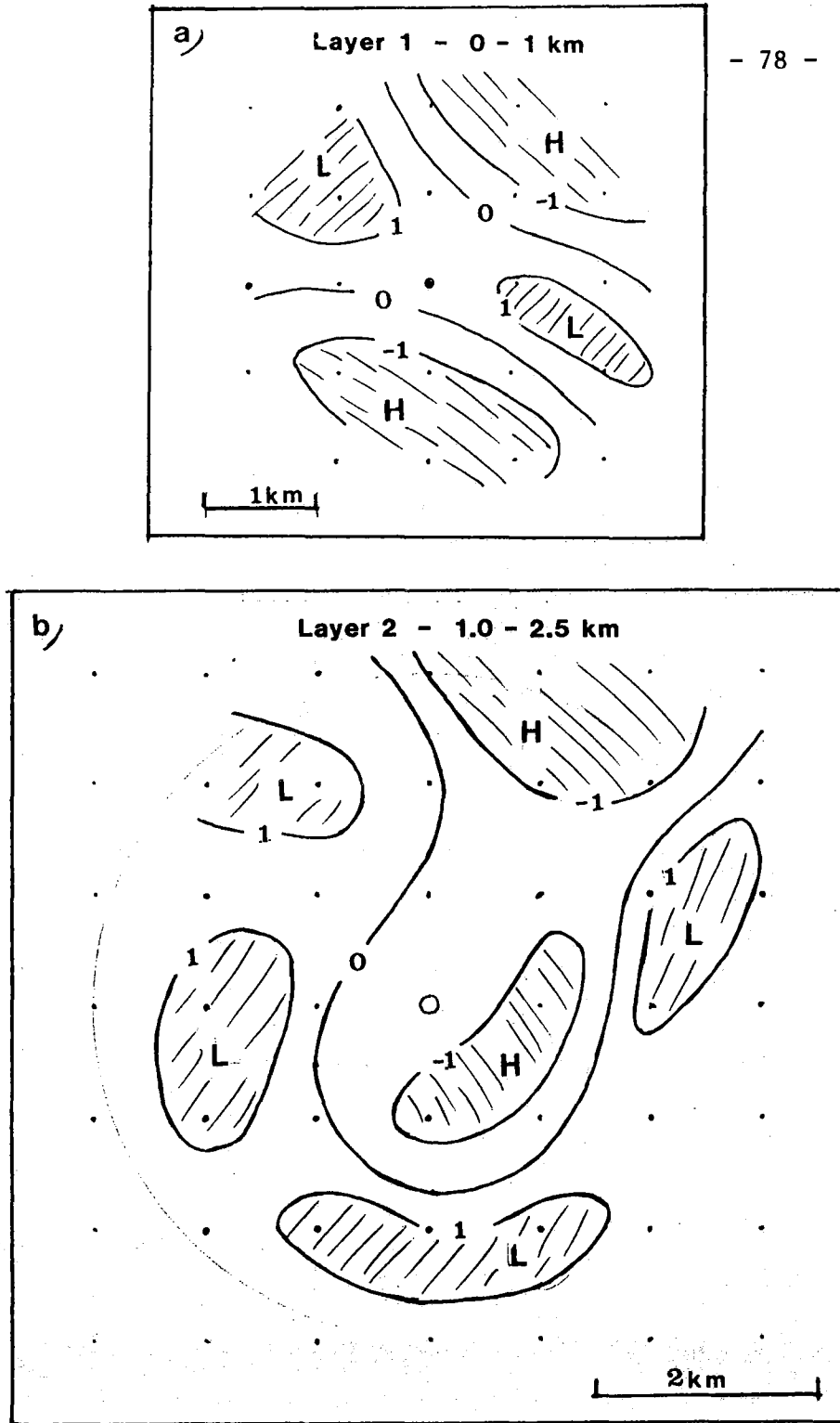


Fig. VII.6.3 Tomographic mapping of NORESS upper crustal structure. Estimated velocity perturbations are of the order of ± 1 per cent; the model "explains" 60% of the variance in the "original" travel time residuals (e.g., see Aki et al, 1977). Interestingly, crustal anomalies beneath NORESS cause significant biases in the estimation of P-wave slowness vectors which are not seen in corresponding estimates using 3-component records. Fig. a) velocity anomalies in layer 1; 0-1 km, block size 0.8 km; H=high and L= low velocities (in per cent) re the average of 5.8 km s^{-1} . Fig. b) velocity anomalies in layer 2; 1.0-2.5 km; block size 1.0 km and average velocity of 6.0 km s^{-1} . Fig. c) velocity anomalies in layer 3; 2.5-5.0 km; block size 1.2 km and average velocity of 6.3 km s^{-1} .

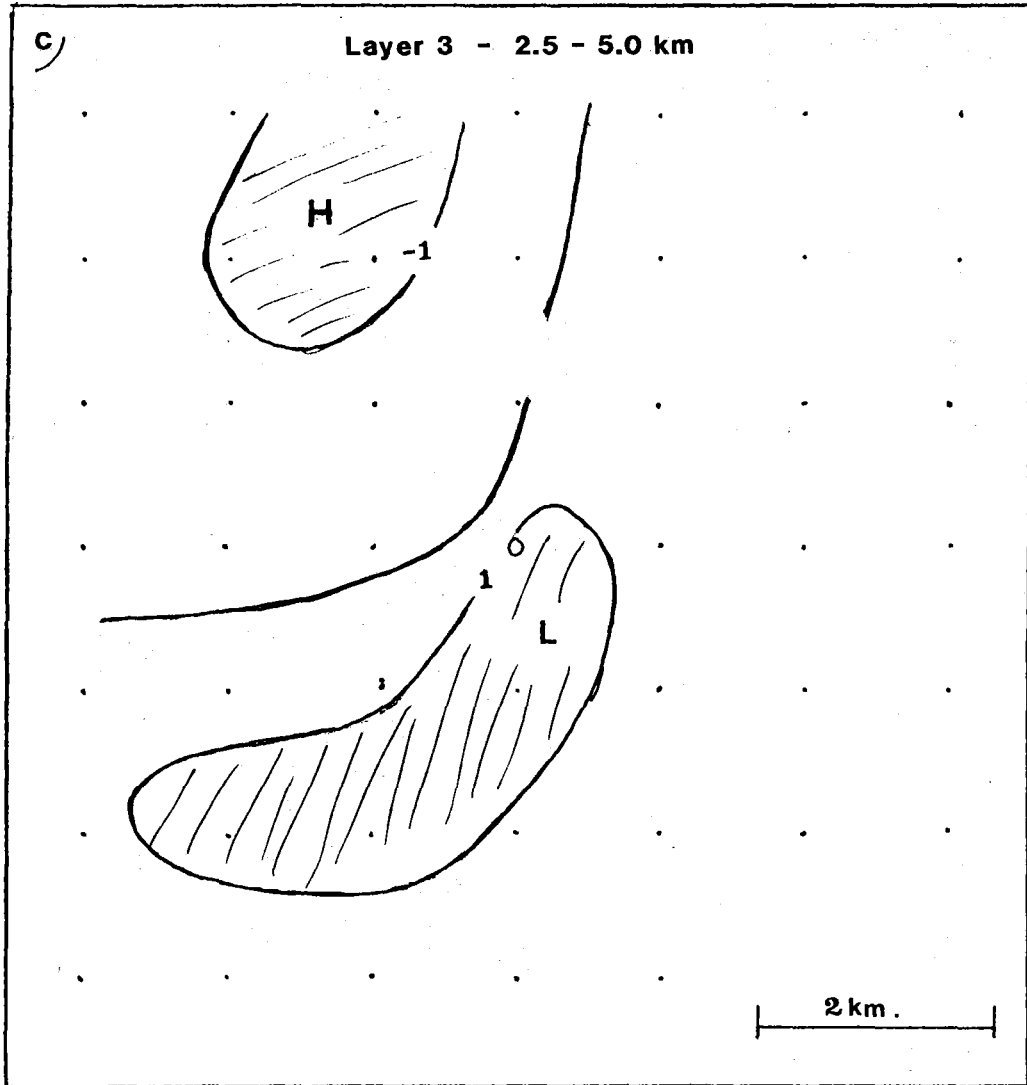


Fig. VII.6.3 (cont.)

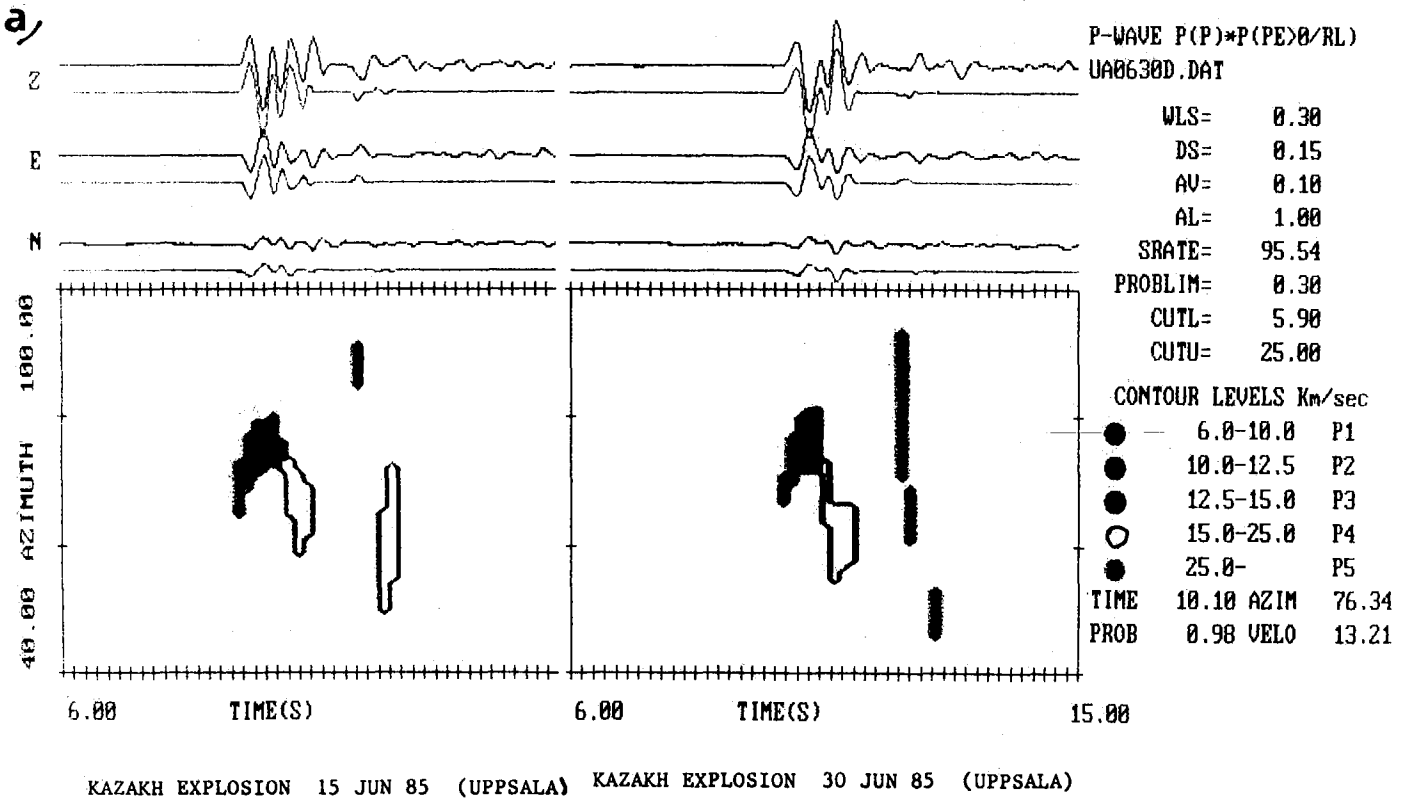


Fig. VII.6.4 Output from 3-component record analysis. Upper traces are original while lower are weight filtered on the basis of estimated P-presence probabilities in the velocity windows of 5.9-25.0 km s⁻¹. Instead of plotting χ^2 -probabilities the corresponding apparent velocities are contoured as a function of time and azimuth. The lower right parameter printouts were "read" from the graphic screen via cursor crosses as indicated. Fig. a) Two nuclear explosions as recorded in Uppsala, Sweden (note similarities in pattern). Fig. b) Hindu Kush earthquake of 4 September 85 (for details, see Table VII.7.2).

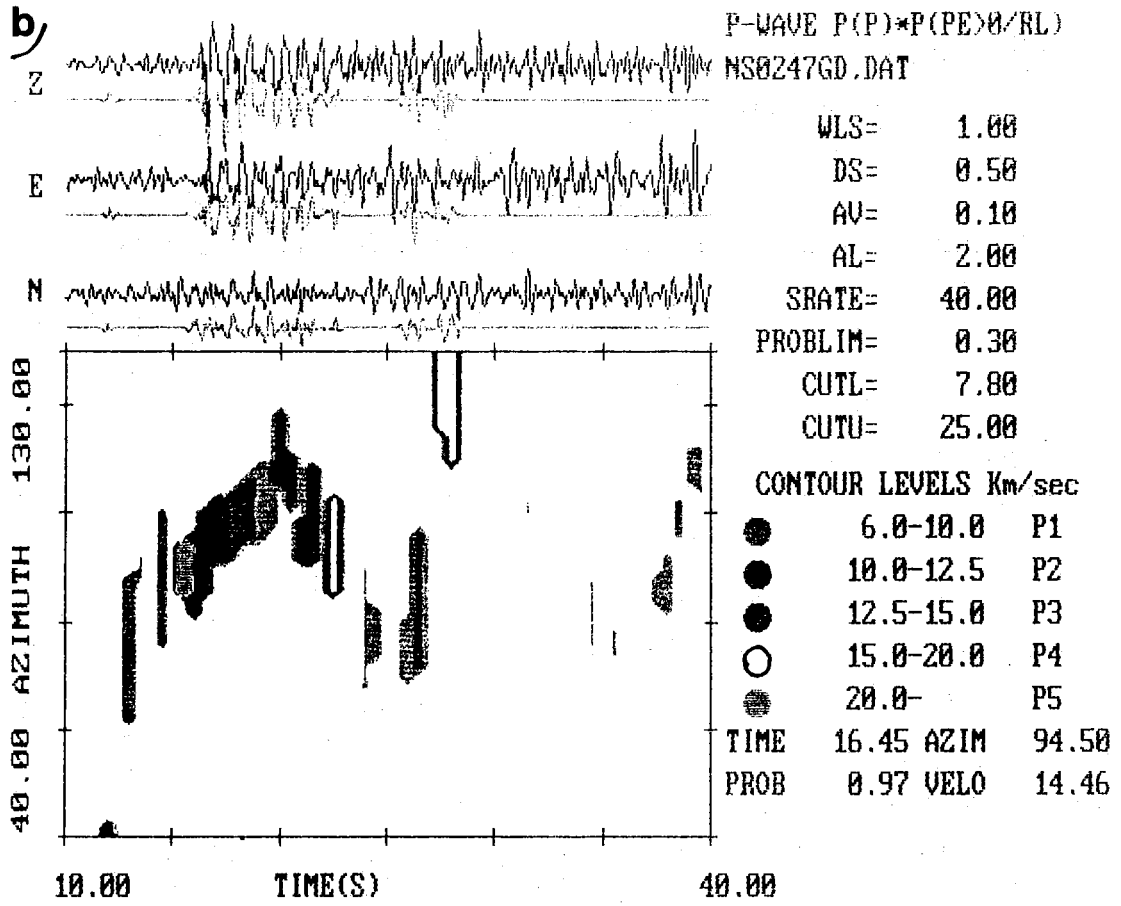


Fig. VII.6.4 (cont.)